

The Effects of Attenuation and Scatter Correction on  
Positron Emission Tomography Quantitation

by

James Thomas Gantt Ward

Graduate Program in Medical Physics  
Duke University

Date: \_\_\_\_\_

Approved:

\_\_\_\_\_  
Timothy Turkington, Supervisor

\_\_\_\_\_  
Robert Reiman

\_\_\_\_\_  
Martin Tornai

Thesis submitted in partial fulfillment of  
the requirements for the degree of  
Master of Science in the Graduate Program in  
Medical Physics in the Graduate School  
of Duke University

2015

ABSTRACT

The Effects of Attenuation and Scatter Correction on  
Positron Emission Tomography Quantitation

by

James Thomas Gantt Ward

Graduate Program in Medical Physics  
Duke University

Date: \_\_\_\_\_

Approved:

\_\_\_\_\_  
Timothy Turkington, Supervisor

\_\_\_\_\_  
Robert Reiman

\_\_\_\_\_  
Martin Tornai

An abstract of a thesis submitted in partial  
fulfillment of the requirements for the degree  
of Master of Science in the Graduate Program in  
Medical Physics in the Graduate School of  
Duke University

2015

Copyright by  
James Thomas Gantt Ward  
2015

## Abstract

X-ray computed tomography (CT) forms the basis for attenuation corrected positron emission tomography (PET) using combined PET/CT scanners. With concerns of high radiation exposure to patients through widespread use of CT, the lowest photon flux that will provide uniform attenuation correction for PET to within 5% over a range of body sizes was investigated. Additionally, clinical uniformity measurements are performed on a uniform phantom, but their results may not be applicable as an estimate of error of hot lesions. PET simulations of variability and localized error were performed with and without hot lesions using a tapering phantom. Images were reconstructed using a variety of fixed and modulated tube-current CT scans and various levels of scatter correction. A physical phantom was designed and scanned to augment the simulation results. Attenuation correction of uniform images was within 5% error when using 120 kVp using a noise index of 50 and 140 kVp using a noise index of 50 for all phantom sizes. Variability with hot lesions was within 5% for scans using 120 kVp and greater than 24 mAs for 21.9 cm and 31.7 cm effective diameters and greater than 48 mAs for 38.5 cm effective diameter. Variability was worse in the background than on hot lesions for poor attenuation correction and poor scatter correction cases. Background error overestimates the error in hot lesions when attenuation correction is biased. Variability was within 5% when estimation of scatter magnitude was within 20% of its

true value both with and without hot lesions. Errors in background due to under and overcorrected scatter lead to an over and underestimate of hot lesion errors, respectively. Physical phantom uniformity was within 5% when using 120 kVp and 10 mAs, albeit with a much smaller phantom size. The background error and its underestimation of lesion error was also measured in the physical phantom.

# Contents

|  |      |
|--|------|
| Abstract .....   | iv   |
| List of Tables .....   | vii  |
| List of Figures .....  | viii |
| List of Abbreviations .....                                    | x    |
| Acknowledgements .....   | xi   |
| 1. Introduction .....  | 1    |
| 2. Methods .....   | 6    |
| 2.1 PET Simulation .....                                       | 6    |
| 2.1.1 Uniform PET .....  | 15   |
| 2.1.2 Non-uniform PET .....                                    | 15   |
| 2.2 Physical Whole Body Phantom .....                          | 18   |
| 3 Results .....  | 23   |
| 3.1 PET Simulation .....                                       | 23   |
| 3.1.1 Uniform PET .....  | 24   |
| 3.1.2 Non-uniform PET with Attenuation Correction Errors ..... | 29   |
| 3.1.3 Non-uniform PET with Scatter Correction Errors .....     | 32   |
| 4 Discussion .....   | 40   |
| 5 Conclusion .....   | 43   |
| References .....   | 44   |

## List of Tables

|   |    |
|---|----|
| Table 1: CT acquisition parameters of the solid tapering phantom.....   | 7  |
| Table 2: Major axis, minor axis, and effective diameter measurements for the solid tapering phantom.....  | 8  |
| Table 3: Scatter fraction as a function of effective diameter in the tapering phantom.....  | 12 |
| Table 4: Reconstruction parameters examined in non-uniform PET simulation.....  | 17 |
| Table 5: Percent error of PET image quantitation due to attenuation correction using 120 kVp CT. Analyzed with full body ROI. ....                                | 25 |
| Table 6: Percent error of PET image quantitation due to attenuation correction using 140 kVp CT. Analyzed with full body ROI. ....                                | 26 |
| Table 7: Percent error of PET image quantitation due to attenuation correction using 120 kVp CT. Analyzed with circular ROI. ....                                 | 26 |
| Table 8: Percent error of PET image quantitation due to attenuation correction using 140 kVp CT. Analyzed with circular body ROI. ....                            | 27 |
| Table 9: Percent variability over scatter corrected PET lesion and background ROI mean due to attenuation correction errors for multiple phantom sizes. ....      | 30 |
| Table 10: Percent variability over non-scatter corrected PET lesion and background ROI mean due to attenuation correction errors for multiple phantom sizes. .... | 30 |
| Table 11: Percent Variability over PET Lesion and Background ROI Mean due to Scatter Correction Errors for multiple phantom sizes. ....                           | 33 |
| Table 12: Percent variability over lesion locations using scatter correction and various attenuation corrections. ....  | 37 |
| Table 13: Variability over lesion locations using no scatter correction and various attenuation corrections. ....   | 37 |
| Table 14: Percent variability over lesion locations using TOF and nonTOF reconstructions. ....  | 39 |

## List of Figures

|   |    |
|---|----|
| Figure 1: Solid tapering phantom with major and minor axes indicated. ....  | 4  |
| Figure 2: Reconstructed CT data of the solid tapering phantom from 120 kVp acquisitions using the indicated fixed current. The profile was taken along the major axis, and the profile scaling is in Hounsfield units. The dip at the edges in the profile is due to the scanner forcing pixels outside the FOV to -3000 HU. .... | 9  |
| Figure 3: Simulated PET with lesions. Shows the 15 simulated lesion locations and one lesionless image for the 21.9 cm diameter. Hot lesion contrast is 8:1. ....   | 11 |
| Figure 4: Flow chart of PET simulation. ....  | 14 |
| Figure 5: Physical Phantom with important features indicated. ....  | 19 |
| Figure 6: Physical whole body phantom reconstructed PET images. The flat top of the lesion in second and fourth column is due to an air bubble. The corresponding dark spot in the background of the last image in those two columns is due to the air bubble's position when the CT data were acquired. ....                     | 22 |
| Figure 7: Simulated PET without lesions attenuation corrected with 120 kVp CT scans using the indicated fixed current. Profile was taken along the major axis of the 38.5 cm effective diameter slice. All profiles are displayed on the same scale. ....   | 24 |
| Figure 8: Simulated uniform PET error for multiple 120 kVp fixed tube-current CTs. Analysis was performed using full-body ROI. ....   | 28 |
| Figure 9: Simulated uniform PET error for multiple 120 kVp fixed tube-current CTs. Analysis was performed using circular ROI. ....  | 28 |
| Figure 10: Correlation of background accuracy to lesion accuracy for PET simulations of phantom effective diameter 21.9 cm using erroneous attenuation correction. ....   | 31 |
| Figure 11: Correlation of background accuracy to lesion accuracy for PET simulations of phantom effective diameter 31.7 cm using erroneous attenuation correction. ....   | 31 |
| Figure 12: Correlation of background accuracy to lesion accuracy for PET simulations of phantom effective diameter 38.5 cm using erroneous attenuation correction. ....   | 32 |

|  |    |
|--|----|
| Figure 13: Correlation of background error to lesion error for PET simulations of phantom effective diameter 21.9 cm using erroneous scatter correction..... | 34 |
| Figure 14: Correlation of background error to lesion error for PET simulations of phantom effective diameter 31.7 cm using erroneous scatter correction..... | 34 |
| Figure 15: Correlation of background error to lesion error for PET simulations of phantom effective diameter 38.5 cm using erroneous scatter correction..... | 35 |
| Figure 16: Correlation of background error to lesion error for the physical phantom using CT with 80 kVp and 4 mAs.....                                      | 38 |
| Figure 17: Correlation of background error to lesion error for the physical phantom with 120 kVp and 4 mAs.....  | 38 |
| Figure 18: Correlation of background error to lesion error for the physical phantom using CT with 120 kVp and 10 mAs.....                                    | 39 |

## List of Abbreviations

|      |   |
|------|---|
| ACR  | American College of Radiology               |
| CT   | Computed tomography                         |
| FBP  | Filtered back projection                    |
| FDG  | Fluorodeoxyglucose                          |
| FOV  | Field of view                               |
| FWHM | Full width at half maximum                  |
| GE   | General Electric                            |
| LSO  | Cerium-doped Lutetium Oxyorthosilicate      |
| LYSO | Cerium-doped Lutetium Yttrium Orthosilicate |
| NI   | Noise Index                                 |
| OSEM | Ordered subset expectation maximization     |
| PET  | Positron emission tomography                |
| ROI  | Region of interest                          |
| SUV  | Standardized uptake value                   |
| TOF  | Time of flight                              |

## Acknowledgements

I would like to give a special thanks to Tim Turkington, my advisor, for helping me put this together, mentoring, and being patient with me. His help and guidance has been invaluable with developing my understanding and appreciation for both the field of nuclear medicine and research as a whole.

Thanks to Martin Tornai for taking the time to serve on my committee.

Thanks to Robert Reiman for taking the time to serve on my committee.

Thanks to Robin Davis for help keeping the physical phantom practical and setting up and acquiring data on the physical phantom as well as allowing me to shadow QC on the PET/CT scanners.

Thanks to James Bowsher for the use of his iterative reconstruction program *spect-map*.

# 1. Introduction

Positron emission tomography (PET) has become a widely utilized functional imaging modality. The combination of x-ray computed tomography (CT) with PET gives both structural and functional information from a single two part scan as well as providing an attenuation map to improve the quality of the PET through attenuation correction. The values generated by PET are frequently examined quantitatively and used to track the progression of disease and treatment.

PET voxel values are typically displayed in terms of standardized uptake values (SUV). SUV in a particular volume is defined in Equation 1, where values are decay corrected.

$$SUV = \frac{\text{radioactive concentration}}{\text{injected activity / body weight}} \quad (1)$$

Since SUV is directly proportional to the radioactivity concentration detected, any error in the SUV can lead to error in patient care. For this study, results were analyzed in terms of radioactive concentration.

Ultimately patient radiation dose from CT is dependent on the number of photons used to acquire images. Recent advances in CT technology and technique, specifically modulating the x-ray tube current as the gantry rotates, have provided the opportunity to lower patient dose while still providing diagnostic quality scans. Modulating the tube current is done because less photon flux is required to achieve the same quality image in smaller parts of the body, such as the neck and legs, while more is

required across the torso and abdomen. General Electric's (GE) algorithm for modulating the x-ray tube-current is called SmartmA, and the user-defined parameter that controls it is called the noise index (NI), and is a value prescribed by a physician or specified in a protocol when scanning a patient. The prescribed NI value approximately equals the resulting standard deviation of voxel values in Hounsfield units at the center of a uniform phantom [1]. Therefore lower NI values correspond to a lower noise image but also deliver dose.

Most patient CTs are of diagnostic quality and have more than enough flux for PET attenuation correction purposes. However some patients only receive a low dose scan intended for PET attenuation correction only. This is relevant when a patient has just had a CT scan and acquiring another would be unnecessary dose or in an exam where CT is not necessarily helpful, such as a brain scan. These scans are of particular interest because they present an opportunity to find the lower threshold scan parameters that do not degrade the PET through poor estimation of attenuation from the body. Since the ultimate goal of CT is to produce a three-dimensional attenuation map, the minimum parameters for uniform CT are a good starting point for the minimum CT parameters to reconstruct uniform PET. A CT becomes biased when detected flux causes integration in the detectors that is comparable to their electronic noise. Fluctuations in electronic noise that result in non-positive values must be increased to allow reconstruction, which introduces the bias. This bias is then passed along to the PET

during attenuation correction. The effect on PET attenuation correction has been investigated through the approach of CT uniformity [2]. We have expanded this analysis to include a computer simulated PET using attenuation correction with biased CT scans.

Evaluation of PET system performance is most frequently done using a cylindrical phantom with a 20 cm diameter. These standard phantoms may be used as a uniform radioactivity distribution or with various inserts. For example, the American College of Radiology (ACR) PET phantom uses a Jaszczak insert, four hot inserts of various contrasts, and three cold inserts of various densities. These phantoms are relatively easy to fill and scan, but are unrealistic. Uniformity across this type of phantom is used as a surrogate to assess image uniformity with non-uniform bodies of many different sizes and shapes.

The first step towards a realistic phantom is moving away from a cylindrical geometry. The solid acrylic tapering phantom as well as the extended PET oval phantom (Data Spectrum Corp, Hillsborough, NC) used in this study use a stadium geometry, which is composed of two semicircles fused to opposite ends of a rectangle [3]. A photograph of the tapering phantom is shown in Figure 1. The tapering phantom achieves its range of sizes by increasing the radii of the semi circles.



**Figure 1: Solid tapering phantom with major and minor axes indicated.**

A major advance in PET technology was the introduction of scintillation crystals capable of time of flight (TOF), specifically Cerium-doped Lutetium Oxyorthosilicate (LSO) and Cerium-doped Lutetium Yttrium Orthosilicate (LYSO), the type of crystal used in the GE Discovery 690 (GE Healthcare, Milwaukee, WI). The implications of this advance allow improved image quality in large bodies [4]. TOF was not a specific focus of this study, but the images reconstructed of the physical phantom utilized the functionality during reconstruction.

Achieving a lower dose CT scan can lead to poor attenuation correction for the PET due to low photon flux through the patient. The effect of poor attenuation corrections on uniform PET images was investigated through simulation where errors were intentionally introduced.

The effect of biased CT and incorrect scatter estimation on the variability and accuracy of PET values both on lesions and in the uniform case was also investigated through simulation and measurement of a physical phantom. More specifically if the variability and accuracy of a uniform phantom predicts variability and accuracy of lesions.

## 2. Methods

### 2.1 PET Simulation

All simulation results are based on existing CT data of the solid, acrylic, tapering phantom [5]. CT scans were performed on the tapering phantom using a GE Discovery 690 PET/CT scanner. Data were acquired using multiple fixed and modulated x-ray tube-currents and applied voltages, which are shown in Table 1. Pitch for all scans was 0.984 and field of view (FOV) was 70 cm. To avoid the increased photon flux through the seams of the acrylic, slices for examination were selected from the midpoints of each slab by thresholding. Since the center of each slab corresponds to a different cross sectional area, the set of examined slices represent a range of body sizes. The body sizes were differentiated by equivalent diameter as calculated in Equation 2.

$$Eq. Diameter = \sqrt{major\ axis \times minor\ axis} \quad (2)$$

Table 2 shows the major and minor axis measurements for the examined sizes, and their respective calculated equivalent diameters. A subset of the CT scans performed on the phantom is pictured in Figure 2.

**Table 1: CT acquisition parameters of the solid tapering phantom.**

| Tube Voltage      |                          |                                     |                   |                          |                                     |
|-------------------|--------------------------|-------------------------------------|-------------------|--------------------------|-------------------------------------|
| 120 kVp           |                          |                                     | 140 kVp           |                          |                                     |
| Tube Current (mA) | Gantry Rotation Time (s) | Current-Rotation time Product (mAs) | Tube Current (mA) | Gantry Rotation Time (s) | Current-Rotation time Product (mAs) |
| 10                | 0.4                      | 4                                   | 10                | 0.4                      | 4                                   |
| 15                | 0.4                      | 6                                   | 15                | 0.4                      | 6                                   |
| 20                | 0.4                      | 8                                   | 20                | 0.4                      | 8                                   |
| 25                | 0.4                      | 10                                  | 30                | 0.4                      | 12                                  |
| 30                | 0.4                      | 12                                  | 40                | 0.4                      | 16                                  |
| 40                | 0.4                      | 16                                  | 50                | 0.4                      | 20                                  |
| 50                | 0.4                      | 20                                  | 60                | 0.4                      | 24                                  |
| 60                | 0.4                      | 24                                  | 70                | 0.4                      | 28                                  |
| 70                | 0.4                      | 28                                  | 85                | 0.4                      | 34                                  |
| 85                | 0.4                      | 34                                  | 100               | 0.4                      | 40                                  |
| 100               | 0.4                      | 40                                  | 120               | 0.4                      | 48                                  |
| 120               | 0.4                      | 48                                  | 150               | 0.4                      | 60                                  |
| 150               | 0.4                      | 60                                  | 170               | 0.4                      | 68                                  |
| 170               | 0.4                      | 68                                  | 200               | 0.4                      | 80                                  |
| 200               | 0.4                      | 80                                  | 250               | 0.4                      | 100                                 |
| 250               | 0.4                      | 100                                 | 300               | 0.4                      | 120                                 |
| 300               | 0.4                      | 120                                 | 300               | 1.0                      | 300                                 |
| 300               | 1.0                      | 300                                 | 350               | 0.4                      | 140                                 |
| 350               | 0.4                      | 140                                 | 400               | 0.4                      | 160                                 |
| 400               | 0.4                      | 160                                 | 400               | 1.0                      | 400                                 |
| 400               | 1.0                      | 400                                 | 500               | 0.4                      | 200                                 |
| 500               | 0.4                      | 200                                 | 500               | 1.0                      | 500                                 |
| 500               | 1.0                      | 500                                 | 600               | 0.4                      | 240                                 |
| 600               | 0.4                      | 240                                 | 750               | 0.4                      | 300                                 |
| 750               | 0.4                      | 300                                 |                   |                          |                                     |
| Noise Index       | Gantry Rotation Time (s) |                                     | Noise Index       | Gantry Rotation Time (s) |                                     |
| 30                | 0.4                      |                                     | 30                | 0.4                      |                                     |
| 50                | 0.4                      |                                     | 50                | 0.4                      |                                     |
| 70                | 0.4                      |                                     | 70                | 0.4                      |                                     |

**Table 2: Major axis, minor axis, and effective diameter measurements for the solid tapering phantom.**

| Effective Diameter | Major Axis | Minor Axis |
|--------------------|------------|------------|
| 19.8 cm            | 25.7 cm    | 15.3 cm    |
| 21.9 cm            | 27.9 cm    | 17.2 cm    |
| 24.6 cm            | 30.6 cm    | 19.7 cm    |
| 27.0 cm            | 32.8 cm    | 22.2 cm    |
| 29.3 cm            | 35.3 cm    | 24.3 cm    |
| 31.7 cm            | 37.5 cm    | 26.8 cm    |
| 34.3 cm            | 40.2 cm    | 29.3 cm    |
| 36.4 cm            | 41.9 cm    | 31.7 cm    |
| 38.5 cm            | 44.1 cm    | 33.6 cm    |
| 40.4 cm            | 46.2 cm    | 35.3 cm    |

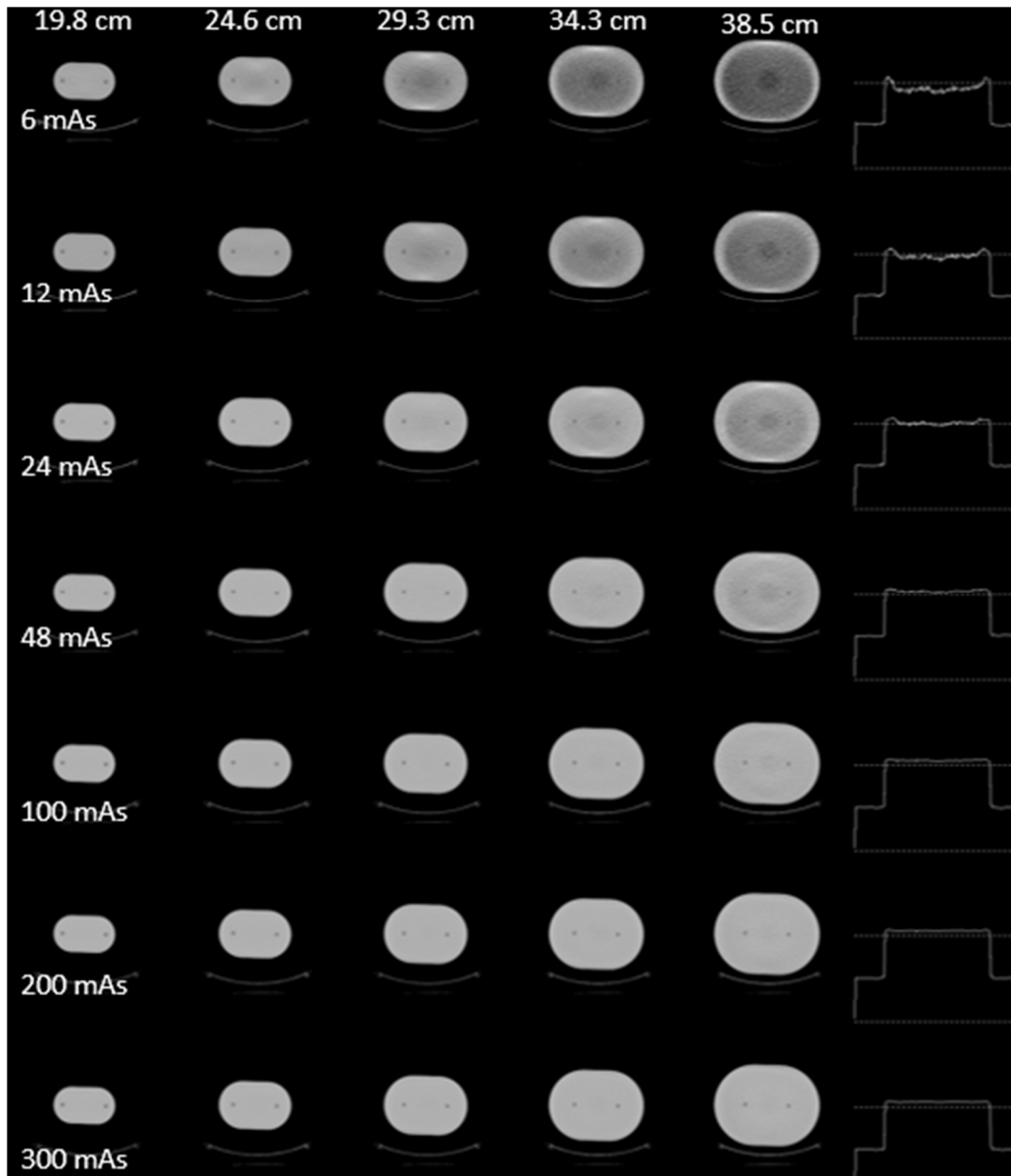
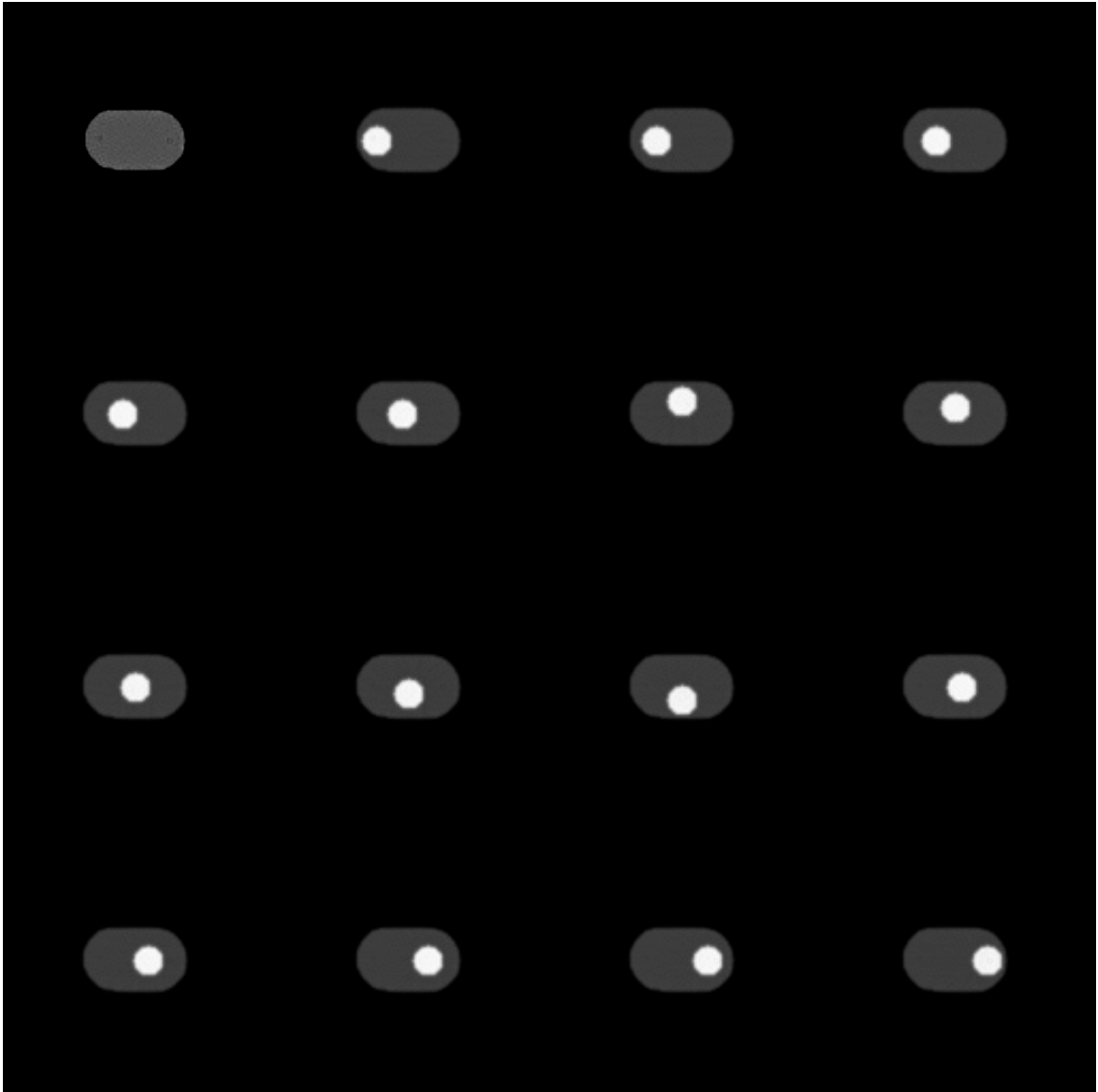


Figure 2: Reconstructed CT data of the solid tapering phantom from 120 kVp acquisitions using the indicated fixed current. The profile was taken along the major axis, and the profile scaling is in Hounsfield units. The dip at the edges in the profile is due to the scanner forcing pixels outside the FOV to -3000 HU.

The reference PET data were generated from the 500 mAs CT scaled down to a 128x128 matrix by pixel averaging. Thresholding was then applied to create a binary image representing the body with 1 and everything else with 0, which limits radioactivity concentration to the body of the phantom. That particular CT was used to avoid nonuniformity of attenuation coefficients in the phantom's center, which allows tighter bounds on the thresholding. In the cases where a hot lesion was added, it was done after the binarizing of the data. Hot lesions were cylindrical with a 7.6 cm diameter to ensure full recovery of reconstructed images for mean-value region of interest (ROI) analysis. A single lesion was added for each simulation at one of fifteen locations along the major and minor axes. Lesion locations are shown in Figure 3. Lesions used a contrast of 8:1. PET data were then forward projected into sinograms.



**Figure 3: Simulated PET with lesions. Shows the 15 simulated lesion locations and one lesionless image for the 21.9 cm diameter. Hot lesion contrast is 8:1.**

An attenuation map was created using the 500 mAs CT to attenuate the projections because it provides the most accurate assessment of attenuation coefficients throughout the phantom. A simulated scatter profile was generated for each projection by convolving a 1D Gaussian with a 10 cm FWHM along each projection [6]. The scatter

fraction, or magnitude of the scatter profile, was scaled by slice as shown in Table 3 [6].

The scatter profile was then added to the PET projections. The scaling was selected based on the scatter fraction measurement in 3D PET. Subtracting the scatter profile from the image served as the scatter correction. Errors were introduced into the scatter correction by rescaling the number of counts by 70%, 80%, 90%, 110%, 120%, and 130% to introduce incorrect scatter estimation. A set of PET data was also generated using no scatter correction at all. The non-scatter corrected simulations were done with a future physical phantom in mind because non-scatter corrected reconstruction is an option on a scanner, which allows for comparison a simulation and measurement of a similar situation. Introducing error by not correcting for scatter is effectively biasing the center of the PET data by adding counts.

**Table 3: Scatter fraction as a function of effective diameter in the tapering phantom.**

| Effective Diameter | Scatter Fraction |
|--------------------|------------------|
| 19.8 cm            | 0.22             |
| 21.9 cm            | 0.25             |
| 24.6 cm            | 0.30             |
| 27.0 cm            | 0.35             |
| 29.3 cm            | 0.43             |
| 31.7 cm            | 0.48             |
| 34.3 cm            | 0.50             |
| 36.4 cm            | 0.53             |
| 38.5 cm            | 0.55             |
| 40.4 cm            | 0.58             |

The PET projections were then attenuation corrected. The PET data were reconstructed using an ordered subset expectation maximization (OSEM) algorithm

using 24 subsets and 2 iterations [7]. After reconstruction, the images were analyzed in two different fashions depending on the result of interest as described below. A flow chart summarizing the main simulation process is shown in Figure 4. Noise was not added to the simulated PET since the primary purpose of this study was to investigate regional biases in the images.

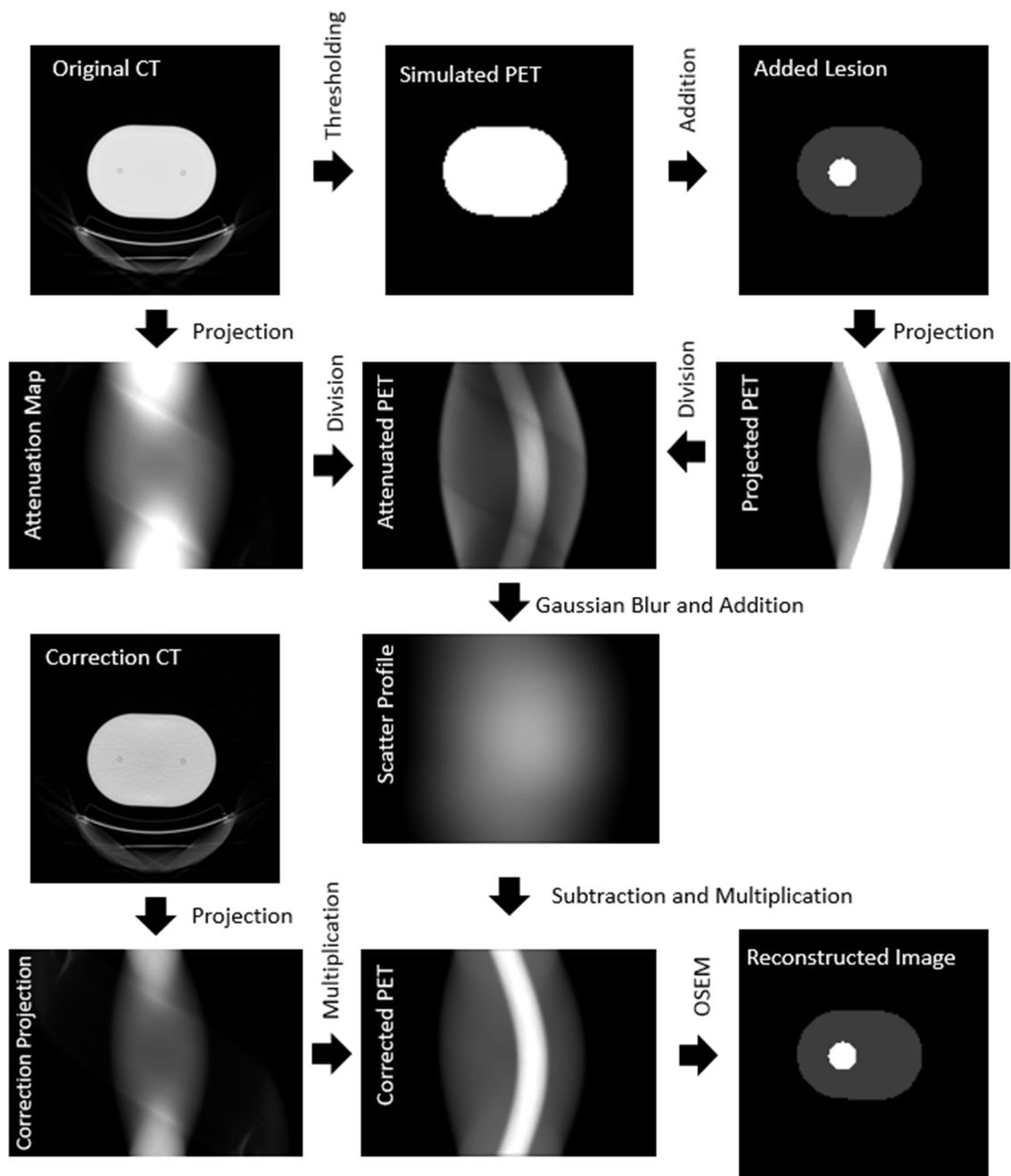


Figure 4: Flow chart of PET simulation.

### 2.1.1 Uniform PET

To analyze the effect of poor attenuation correction on the reconstructed PET images, two sets of ROIs were generated. A circular ROI with a diameter 4.9 cm was placed at the center of the phantom, and a full-body ROI was generated by thresholding around the edge of the phantom for each body size and removing 2.2 cm from the edges of the ROI to avoid edge artifacts. The mean pixel values of these ROIs over the range of phantom sizes were examined. Reference values were determined by the results from the PET reconstruction using the 500 mAs CT for attenuation and attenuation correction. This is the ideal reconstruction in that the attenuation is exactly corrected, and it yields zero error in analysis. Analysis criteria were set such that less than 5% error from the reference was considered to be an acceptably accurate correction. Error was calculated as shown in Equation 3, where  $\bar{x}$  is the mean value in the ROI of a poorly corrected reconstruction.

$$\text{Percent Error} = 100\% \times \left( \frac{\text{reference} - \bar{x}}{\text{reference}} \right) \quad (3)$$

The full set of CT scans was used when performing this analysis.

### 2.1.2 Non-uniform PET

For the uniformity analysis, a PET image reconstructed using the ideal attenuation and scatter corrections was used as the reference for each lesion location. The point of this analysis is to determine if the degree of uniformity in the lesionless image implies the same variability in hot lesions. Analysis was done on three different

phantom sizes, effective diameters of 21.9 cm, 31.7 cm, and 38.5 cm. These sizes were selected to roughly correspond with perimeters of 30, 40, and 50 inches to represent a range of adult patient abdomen sizes. Uniformity was examined by perturbations in a single effect, either errant attenuation or scatter correction. Using a set of circular ROIs with a 4.4 cm diameter centered on each lesion, the effect of image nonuniformity on hot lesion variability was examined in two different ways.

First, the mean voxel value of each ROI location was determined. The standard deviation of these means was calculated as a percentage of the mean to quantify how much variability existed over the examined regions. Variability calculation is shown in Equation 4 where  $\sigma_{\bar{x}}$  is the standard deviation of means, and  $\bar{\bar{x}}$  is the mean of the means. Variability was calculated according to Equation 4.

$$Variability = 100\% \times \left( \frac{\sigma_{\bar{x}}}{\bar{\bar{x}}} \right) \quad (4)$$

Second, the value of each ROI with no lesion present was divided by the expected value for that ROI as determined by the ideal reconstruction. Similarly, the same ratio was calculated for the hot lesions. The error of location  $i$  was calculated by Equation 5.

$$Error_i = \frac{measured_i}{expected_i} \quad (5)$$

A scatter plot was generated for the error both with and without lesions, and linear regression was performed. The line was set to have an intercept of zero, and the slope of the line was compared to 1. A slope of 1 would indicate that any error without a lesion

would indicate the same level of error when a lesion is present. A slope of less than 1 would indicate that error when lesions are present is overestimated by background error. Similarly, a slope of greater than 1 indicates on-lesion error is underestimated by background error. Both variability and error were examined for 7 different CT scan parameters and 7 different scatter correction levels shown in Table 4.

**Table 4: Reconstruction parameters examined in non-uniform PET simulation.**

| Attenuation Correction: 120 kVp | Scatter Correction Scaling |
|---------------------------------|----------------------------|
| 24 mAs                          | No correction              |
| 48 mAs                          | 60%                        |
| 100 mAs                         | 80%                        |
| 200 mAs                         | 90%                        |
| 300 mAs                         | 110%                       |
| 400 mAs                         | 120%                       |
| 500 mAs                         | 140%                       |

This analysis was conducted on contrast of 8:1. For uniformity after incorrect attenuation correction, a biased CT using 120 kVp and 24 mAs was selected to provide results over a range of background accuracies based on the results of the uniform PET simulation. The PET was reconstructed both with and without scatter correction in this case. When examining erroneous scatter correction, scatter profile scaling of 80% and 120% were examined with regression after reconstructing the PET using a CT with 120 kVp and 400 mAs.

## **2.2 Physical Whole Body Phantom**

In order to verify the results obtained from simulation, a physical phantom was constructed using half of the extended PET oval phantom. The acrylic phantom has a major axis of 34 cm and minor axis of 19 cm leading to an effective diameter of 25.4 cm. An acrylic pegboard with threaded holes was mounted to the bottom of the phantom at its midpoint using electrical tape as shown in Figure 5. Two 250 mL low density polyethylene cylindrical bottles of diameter 5.8 cm were fitted with a nylon bolt through the cap so they could be screwed into the pegboard and moved to different locations. A bottle was mounted on each side of the pegboard so each side would only have a single cylindrical hot lesion.

The bottles and phantom were filled with a solution of Fluorodeoxyglucose (FDG) in water at a ratio of 9.60:1. A total activity of 0.41 mCi in each bottle and 4.09 mCi in the background was used. Due to the presence of the pegboard restricting circulation through the phantom, both top fill ports were used in an attempt to evenly distribute the radioactive background solution. The CT and PET scans were performed with a GE Discovery 690 PET/CT scanner. The CT was acquired with a pitch of 0.984 and 0.4 s gantry rotation period.

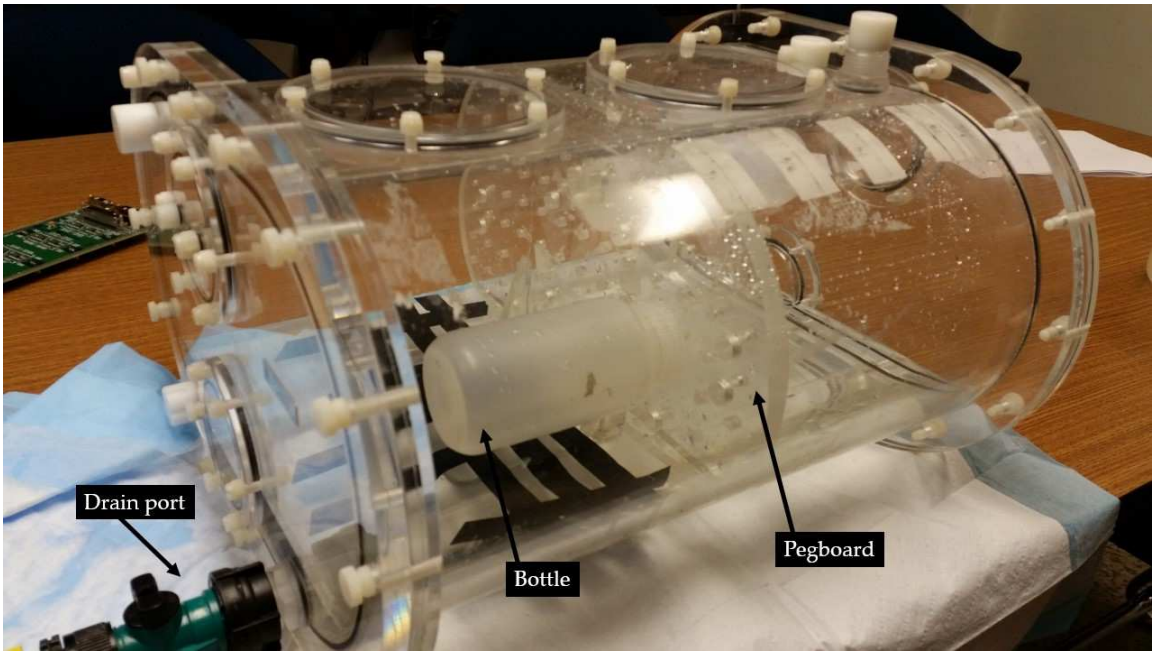


Figure 5: Physical Phantom with important features indicated.

Two PET scans were performed on the phantom. Each scan used two bed positions with 6 minutes of acquisition each. Each bed position was centered on a bottle to give the highest sensitivity to the hot lesion. Between the scans, the phantom was partially drained using an attached stopcock valve and tube, and the bottles containing the concentrated FDG were moved to different positions on the pegboard before refilling the phantom with the same radioactive water. This process resulted in a total of four lesion locations.

Four CTs were acquired of the phantom: 80 kVp with 4 mAs and 120 kVp with 4 mAs, 10 mAs, and 48 mAs. The CT data were only acquired for a single orientation of the bottles corresponding to the first PET scan. This led to a small artifact in the background of the second PET acquisition due to an air bubble present in one of the bottles.

The PET acquisitions were reconstructed using the set of attenuation corrections both with and without scatter correction. All reconstructions used OSEM iterative reconstruction with 24 subsets and 2 iterations as well as the TOF capability. PET images reconstructed by the system used a 50 cm FOV on a 128x128 grid with 83 axial slices. Well counter, uniformity, dead-time, and random corrections were applied. A single PET acquisition was reconstructed using the 120 kVp with 48 mAs CT for attenuation correction both with and without the TOF capability.

A 3.9 cm diameter circular ROI was placed in the center of each hot lesion to measure a mean value. The smaller ROI in this analysis compared to the simulation was due to the smaller lesion size. The mean data from five adjacent slices were used for analysis to provide a larger sampling of points. Axially, the five slices were selected around the bottle's midpoint. Figure 6 shows some of the images acquired of the physical phantom reconstructed several different ways.

Analysis was similar to that from the non-uniform simulation. The variability analysis was done in exactly the same manner. The error correlation was conducted over a series of different attenuation corrections instead of body sizes due to the fixed size of the phantom.

An important note for the analysis of the physical phantom is that no uniform, lesionless area was scanned. The lesionless data are acquired from regions away from the hot lesions, but in the same axial slice. This was done because no scan was performed without the bottles inserted and the bed positions did not extend past the end of the bottles.

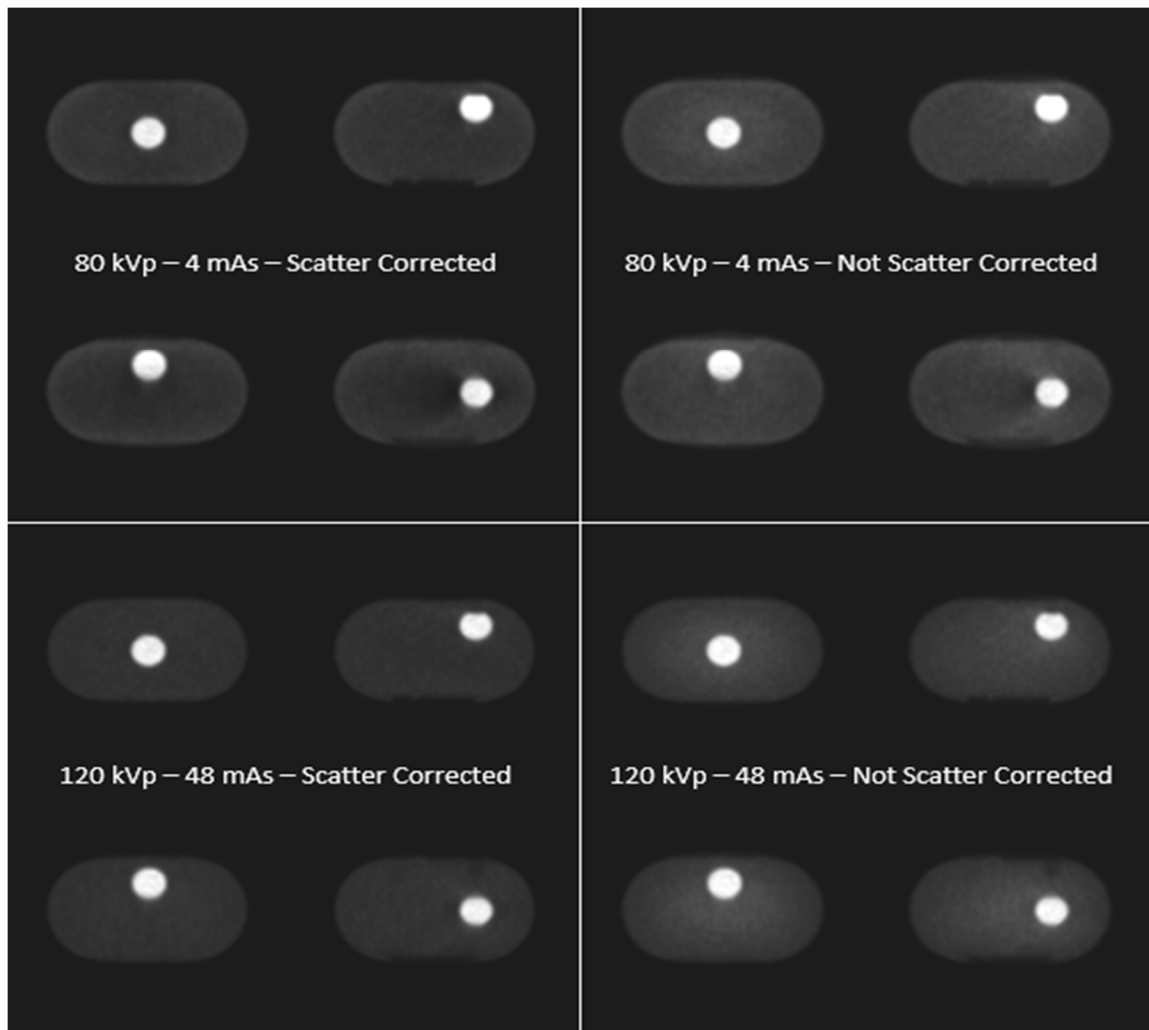


**Figure 6: Physical whole body phantom reconstructed PET images. The flat top of the lesion in second and fourth column is due to an air bubble. The corresponding dark spot in the background of the last image in those two columns is due to the air bubble's position when the CT data were acquired.**

## **3 Results**

### ***3.1 PET Simulation***

Through the use of the tapering phantom, simulation results were gathered for a range of body sizes. Reconstructed simulated PET images using a series of attenuation corrections with no added lesions are pictured in Figure 7.

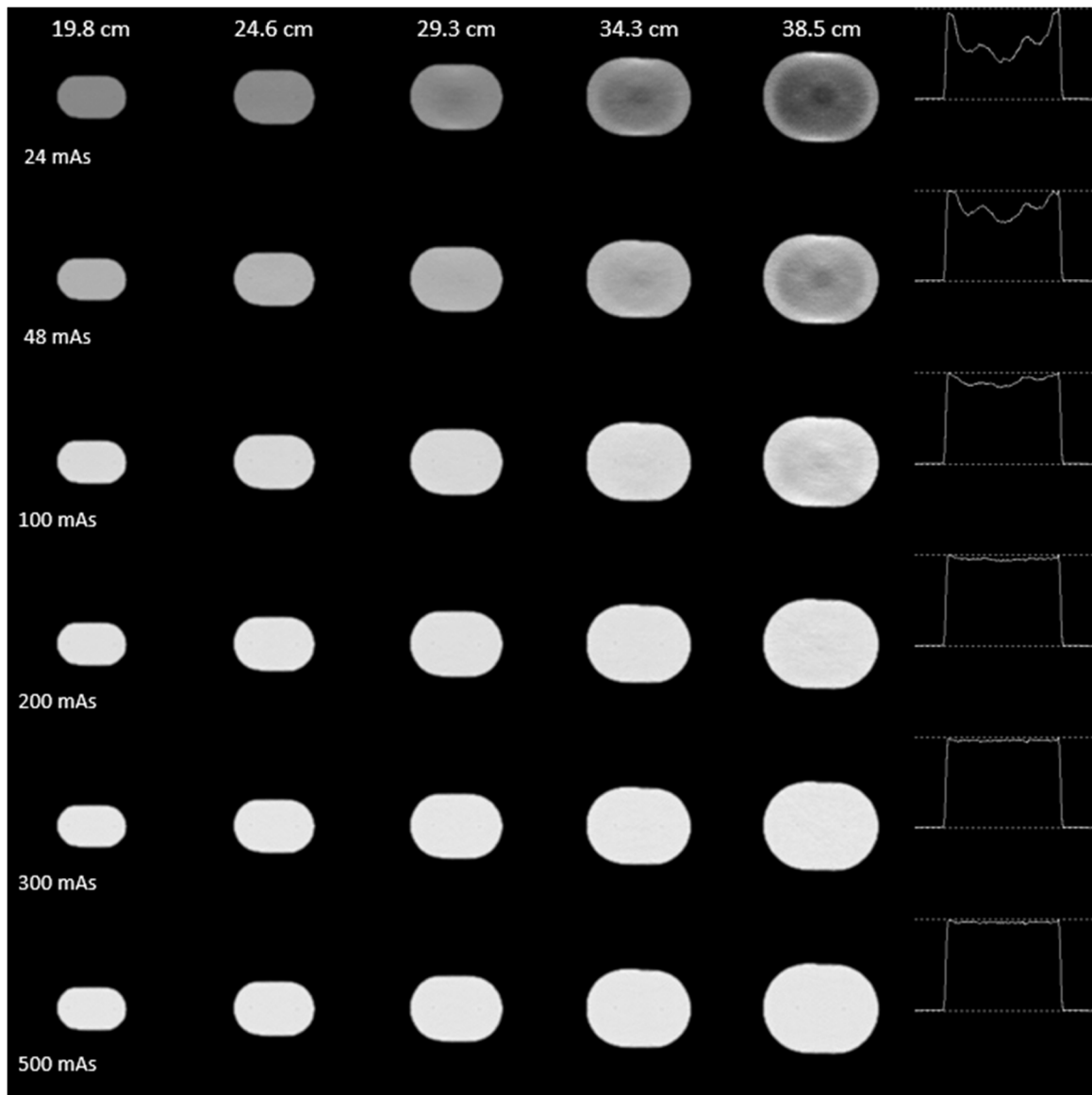


**Figure 7: Simulated PET without lesions attenuation corrected with 120 kVp CT scans using the indicated fixed current. Profile was taken along the major axis of the 38.5 cm effective diameter slice. All profiles are displayed on the same scale.**

### 3.1.1 Uniform PET

As the results in Tables 5-8 show, the series of fixed tube-current scans combined with the range of phantom sizes show that there is a minimum tube current above which

the correction to PET only marginally improves, but dose continues to increase. The analysis with the circular ROI indicates that the errors are worse at the center of the phantom as expected by after looking at a profile through the simulated PET reconstructions. This result is plotted for the 120 kVp corrections in Figures 8-9. The modulated current scans produced errors that varied less with body size than the fixed current scans because of the increased current applied as the phantom increased in size. Based on the results, a NI of 50 for kVp of 120 or 140 limits error to within 5% in the worst case at the center of the phantom. Therefore, NI of 50 provides the minimum dose while maintaining image quality necessary for PET quantitation within 5%.

**Table 5: Percent error of PET image quantitation due to attenuation correction using 120 kVp CT. Analyzed with full body ROI.**

| Fixed Current     | Effective Phantom Diameter (cm) |        |        |        |        |        |        |        |
|-------------------|---------------------------------|--------|--------|--------|--------|--------|--------|--------|
|                   | 19.8                            | 21.9   | 24.6   | 27     | 29.3   | 31.7   | 34.3   | 36.4   |
| 4 mAs             | -1.00%                          | 4.05%  | 8.64%  | 19.77% | 29.06% | 39.35% | 49.24% | 56.21% |
| 8 mAs             | 0.37%                           | -0.21% | 3.41%  | 7.37%  | 16.96% | 25.38% | 34.32% | 44.09% |
| 12 mAs            | 0.63%                           | -0.35% | 1.52%  | 3.73%  | 10.57% | 17.84% | 26.04% | 35.63% |
| 20 mAs            | 0.51%                           | -0.42% | -0.26% | 2.15%  | 4.44%  | 9.79%  | 16.72% | 24.00% |
| 40 mAs            | -0.35%                          | -0.32% | -0.10% | 0.25%  | 0.83%  | 2.89%  | 6.53%  | 11.48% |
| 80 mAs            | 0.36%                           | -0.73% | -0.88% | 0.30%  | -0.06% | 0.53%  | 1.21%  | 4.14%  |
| 160 mAs           | -0.44%                          | 0.08%  | 0.23%  | 0.18%  | -0.03% | 0.02%  | 0.27%  | 0.83%  |
| 500 mAs           | 0.00%                           | 0.00%  | 0.00%  | 0.00%  | 0.00%  | 0.00%  | 0.00%  | 0.00%  |
| Modulated Current |                                 |        |        |        |        |        |        |        |
| 30 NI             | 0.93%                           | 0.82%  | 0.27%  | 1.74%  | 1.21%  | 1.46%  | 1.73%  | 1.71%  |
| 50 NI             | 0.70%                           | 1.10%  | 0.94%  | 1.30%  | 1.43%  | 1.65%  | 2.33%  | 1.93%  |
| 70 NI             | 0.62%                           | 1.07%  | 1.39%  | 1.58%  | 2.25%  | 2.73%  | 3.81%  | 4.79%  |

**Table 6: Percent error of PET image quantitation due to attenuation correction using 140 kVp CT. Analyzed with full body ROI.**

| Fixed Current     | Effective Phantom Diameter (cm) |        |        |        |        |        |        |        |
|-------------------|---------------------------------|--------|--------|--------|--------|--------|--------|--------|
|                   | 19.8                            | 21.9   | 24.6   | 27     | 29.3   | 31.7   | 34.3   | 36.4   |
| 4 mAs             | 0.11%                           | -0.53% | 4.31%  | 8.30%  | 19.09% | 27.83% | 36.79% | 46.83% |
| 8 mAs             | 0.74%                           | -0.68% | 0.55%  | 2.07%  | 8.16%  | 14.50% | 22.19% | 31.78% |
| 12 mAs            | 0.48%                           | -0.47% | -0.38% | 1.52%  | 3.55%  | 8.43%  | 15.19% | 22.12% |
| 20 mAs            | 0.51%                           | -0.77% | -0.76% | 0.70%  | 0.98%  | 3.73%  | 7.32%  | 13.06% |
| 40 mAs            | 0.44%                           | -0.62% | -0.77% | 0.36%  | 0.02%  | 0.71%  | 1.84%  | 4.72%  |
| 80 mAs            | 0.25%                           | -0.68% | -0.73% | 0.10%  | -0.44% | -0.18% | -0.25% | 0.90%  |
| 160 mAs           | 0.91%                           | 0.08%  | 0.29%  | -0.01% | -0.34% | -0.27% | -0.12% | 0.10%  |
| 500 mAs           | 0.00%                           | 0.00%  | 0.00%  | 0.00%  | 0.00%  | 0.00%  | 0.00%  | 0.00%  |
| Modulated Current |                                 |        |        |        |        |        |        |        |
| 30 NI             | -0.33%                          | -0.20% | -0.59% | -0.21% | -0.49% | -0.39% | 0.05%  | -1.02% |
| 50 NI             | -0.90%                          | -0.57% | -1.38% | 0.35%  | -0.20% | 0.15%  | 0.28%  | -0.32% |
| 70 NI             | -0.74%                          | -0.57% | -0.38% | -0.24% | 0.14%  | 0.52%  | 1.26%  | 1.07%  |

**Table 7: Percent error of PET image quantitation due to attenuation correction using 120 kVp CT. Analyzed with circular ROI.**

| Fixed Current     | Effective Phantom Diameter (cm) |        |        |        |        |        |        |        |
|-------------------|---------------------------------|--------|--------|--------|--------|--------|--------|--------|
|                   | 19.8                            | 21.9   | 24.6   | 27     | 29.3   | 31.7   | 34.3   | 36.4   |
| 4 mAs             | 5.50%                           | 29.88% | 41.95% | 55.88% | 66.62% | 74.49% | 81.17% | 84.55% |
| 8 mAs             | -0.30%                          | 12.66% | 25.06% | 36.06% | 50.48% | 60.92% | 68.93% | 75.74% |
| 12 mAs            | -1.45%                          | 6.33%  | 15.83% | 25.07% | 38.85% | 50.31% | 59.07% | 67.83% |
| 20 mAs            | -0.42%                          | 1.04%  | 5.72%  | 14.35% | 23.72% | 34.25% | 45.44% | 53.56% |
| 40 mAs            | -0.69%                          | -1.72% | 0.19%  | 3.45%  | 8.38%  | 15.22% | 23.57% | 32.99% |
| 80 mAs            | 0.14%                           | -1.24% | -1.66% | -0.07% | 1.21%  | 4.05%  | 7.60%  | 14.94% |
| 160 mAs           | -0.40%                          | -0.26% | 0.03%  | -0.30% | 0.06%  | 0.31%  | 1.02%  | 3.60%  |
| 500 mAs           | 0.00%                           | 0.00%  | 0.00%  | 0.00%  | 0.00%  | 0.00%  | 0.00%  | 0.00%  |
| Modulated Current |                                 |        |        |        |        |        |        |        |
| 30 NI             | 0.69%                           | 1.05%  | -0.20% | 1.83%  | 1.09%  | 1.44%  | 1.68%  | 2.44%  |
| 50 NI             | -0.24%                          | 0.53%  | 1.42%  | 1.40%  | 2.20%  | 2.58%  | 3.37%  | 4.20%  |
| 70 NI             | 3.43%                           | 3.59%  | 7.18%  | 4.90%  | 6.93%  | 8.55%  | 9.91%  | 14.27% |

**Table 8: Percent error of PET image quantitation due to attenuation correction using 140 kVp CT. Analyzed with circular body ROI.**

| Fixed Current     | Effective Phantom Diameter (cm) |        |        |        |        |        |        |        |
|-------------------|---------------------------------|--------|--------|--------|--------|--------|--------|--------|
|                   | 19.8                            | 21.9   | 24.6   | 27     | 29.3   | 31.7   | 34.3   | 36.4   |
| 4 mAs             | 0.64%                           | 15.31% | 29.28% | 39.85% | 54.32% | 64.46% | 72.15% | 78.83% |
| 8 mAs             | -1.03%                          | 4.08%  | 11.97% | 21.05% | 34.61% | 45.43% | 54.91% | 64.02% |
| 12 mAs            | -0.33%                          | 0.40%  | 5.18%  | 13.04% | 22.10% | 32.13% | 43.46% | 51.96% |
| 20 mAs            | 0.12%                           | -2.21% | 0.26%  | 4.99%  | 10.50% | 18.10% | 27.40% | 36.50% |
| 40 mAs            | 0.32%                           | -1.34% | -1.62% | 0.37%  | 2.10%  | 5.17%  | 10.11% | 16.42% |
| 80 mAs            | 0.14%                           | -1.07% | -1.17% | -0.51% | -0.44% | 0.24%  | 1.29%  | 4.68%  |
| 160 mAs           | 0.86%                           | -0.13% | 0.36%  | -0.42% | -0.28% | -0.34% | -0.06% | -0.02% |
| 500 mAs           | 0.00%                           | 0.00%  | 0.00%  | 0.00%  | 0.00%  | 0.00%  | 0.00%  | 0.00%  |
| Modulated Current |                                 |        |        |        |        |        |        |        |
| 30 NI             | -0.60%                          | -0.34% | -1.00% | -0.38% | -0.47% | -0.63% | -0.07% | -1.46% |
| 50 NI             | -2.68%                          | -1.23% | -2.14% | 0.33%  | -0.27% | 0.42%  | 0.56%  | 0.58%  |
| 70 NI             | -1.01%                          | -0.68% | 2.42%  | 0.93%  | 2.92%  | 4.16%  | 4.67%  | 6.59%  |

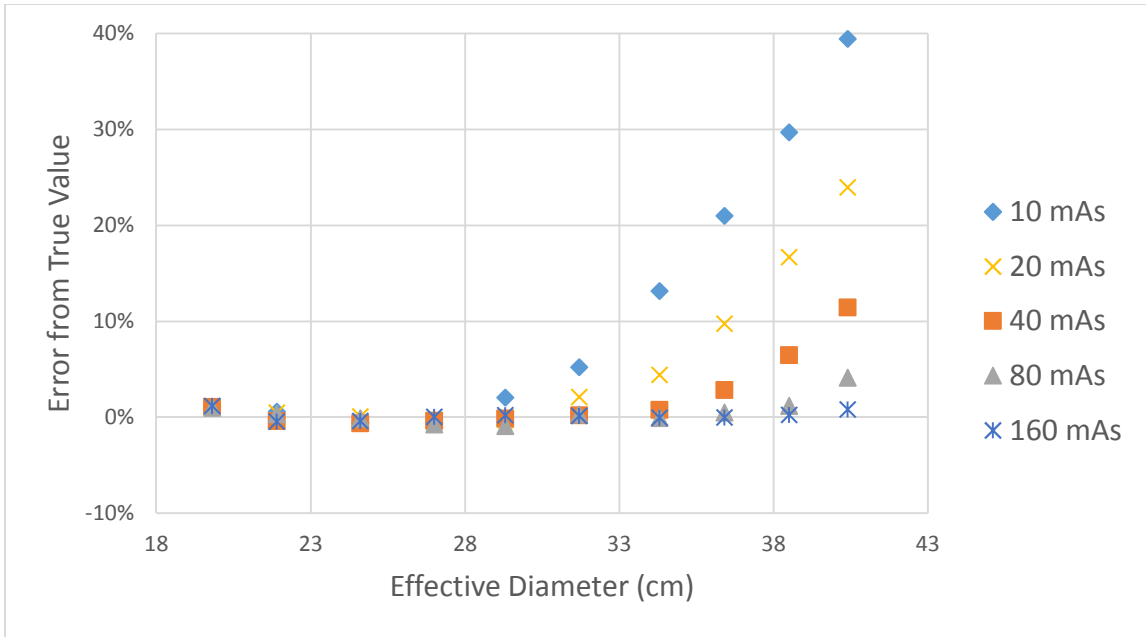


**Figure 8: Simulated uniform PET error for multiple 120 kVp fixed tube-current CTs. Analysis was performed using full-body ROI.**

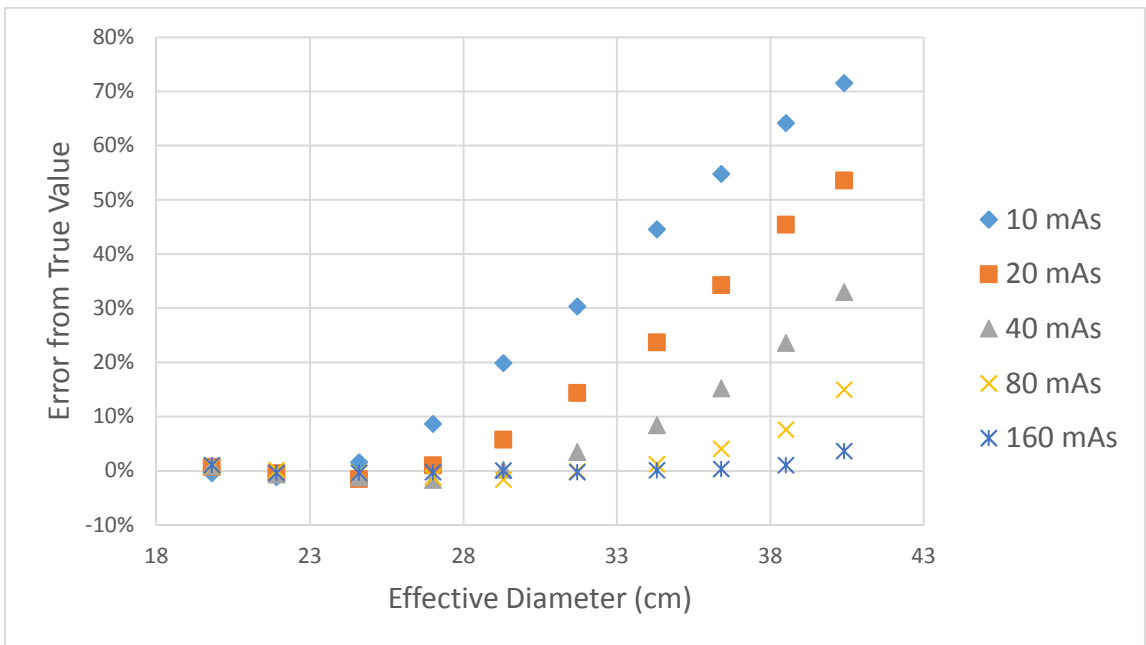


**Figure 9: Simulated uniform PET error for multiple 120 kVp fixed tube-current CTs. Analysis was performed using circular ROI.**

### 3.1.2 Non-uniform PET with Attenuation Correction Errors

As with the uniform images, quantitative PET error decreased as the attenuation correction improved. The percent variability in scatter corrected and incorrectly attenuation corrected PET images was higher in the uniform image. Simulated PET variability across the image decreased with increasing tube current. As shown in Tables 9-10, variability was within 3% for both 8:1 and background (1:1) contrast at and above 120 kVp CT with 100 mAs for the largest body size. For non-scatter corrected PET images with incorrect attenuation correction, overall variability was higher for the 8:1 contrast, but not for the 1:1 contrast.

As shown in Figures 10-12, applying linear regression to examine error over various body sizes shows that background and on-lesion errors are similar to within 3% of unit slope, which means that over and underestimations are to within 3%. Error of hot lesions is overestimated for the 21.9 cm diameter, but is underestimated for the 31.7 cm and 38.5 cm sizes. Error with and without scatter corrections are similar in every case, even when error is high as in the 38.5 cm diameter case. The lower error for the non-scatter corrected simulation at the larger body size is due to the correcting effect of the added counts in the biased region of the PET.

**Table 9: Percent variability over scatter corrected PET lesion and background ROI mean due to attenuation correction errors for multiple phantom sizes.**

|               | Effective Diameter |       |         |       |         |        |
|---------------|--------------------|-------|---------|-------|---------|--------|
|               | 21.9 cm            |       | 31.7 cm |       | 38.5 cm |        |
| Fixed Current | 8:1                | 1:1   | 8:1     | 1:1   | 8:1     | 1:1    |
| 24 mAs        | 0.18%              | 0.26% | 1.26%   | 2.94% | 3.38%   | 10.07% |
| 48 mAs        | 0.19%              | 0.25% | 0.20%   | 0.59% | 1.49%   | 4.31%  |
| 100 mAs       | 0.13%              | 0.14% | 0.22%   | 0.22% | 0.55%   | 1.54%  |
| 200 mAs       | 0.18%              | 0.23% | 0.17%   | 0.20% | 0.18%   | 0.26%  |
| 300 mAs       | 0.13%              | 0.16% | 0.08%   | 0.17% | 0.14%   | 0.11%  |
| 400 mAs       | 0.11%              | 0.16% | 0.09%   | 0.23% | 0.11%   | 0.18%  |
| 500 mAs       | 0.10%              | 0.14% | 0.09%   | 0.21% | 0.09%   | 0.08%  |

**Table 10: Percent variability over non-scatter corrected PET lesion and background ROI mean due to attenuation correction errors for multiple phantom sizes.**

|               | Effective Diameter |       |         |       |         |       |
|---------------|--------------------|-------|---------|-------|---------|-------|
|               | 21.9 cm            |       | 31.7 cm |       | 38.5 cm |       |
| Fixed Current | 8:1                | 1:1   | 8:1     | 1:1   | 8:1     | 1:1   |
| 24 mAs        | 1.18%              | 6.43% | 0.66%   | 6.04% | 2.33%   | 3.82% |
| 48 mAs        | 1.21%              | 6.39% | 1.69%   | 7.72% | 0.61%   | 2.35% |
| 100 mAs       | 1.06%              | 6.25% | 1.98%   | 8.07% | 0.95%   | 3.83% |
| 200 mAs       | 1.19%              | 6.37% | 1.94%   | 7.98% | 1.49%   | 4.74% |
| 300 mAs       | 1.13%              | 6.32% | 1.88%   | 7.94% | 1.45%   | 4.69% |
| 400 mAs       | 1.12%              | 6.30% | 1.85%   | 7.88% | 1.42%   | 4.66% |
| 500 mAs       | 1.10%              | 6.28% | 1.86%   | 7.90% | 1.42%   | 4.63% |

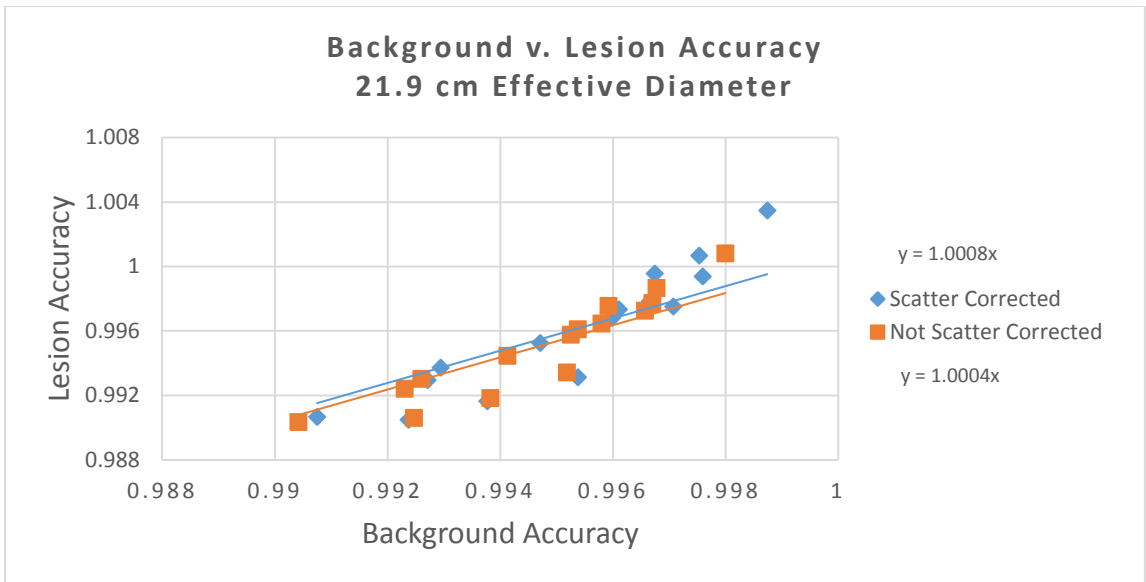


**Figure 10: Correlation of background accuracy to lesion accuracy for PET simulations of phantom effective diameter 21.9 cm using erroneous attenuation correction.**

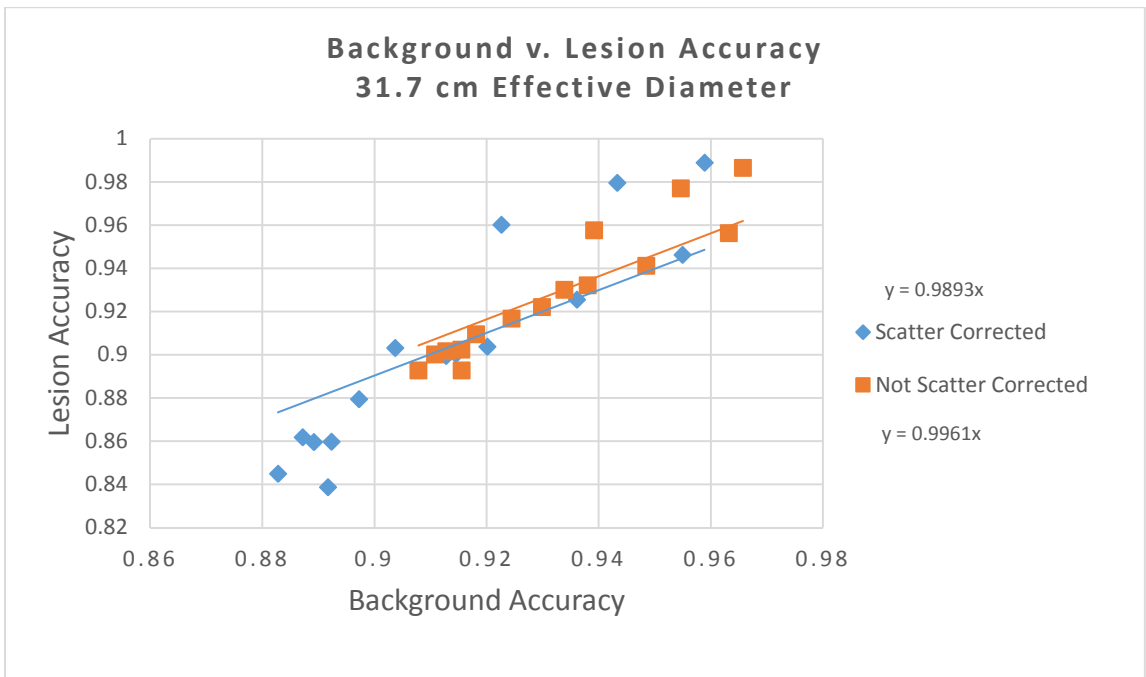


**Figure 11: Correlation of background accuracy to lesion accuracy for PET simulations of phantom effective diameter 31.7 cm using erroneous attenuation correction.**

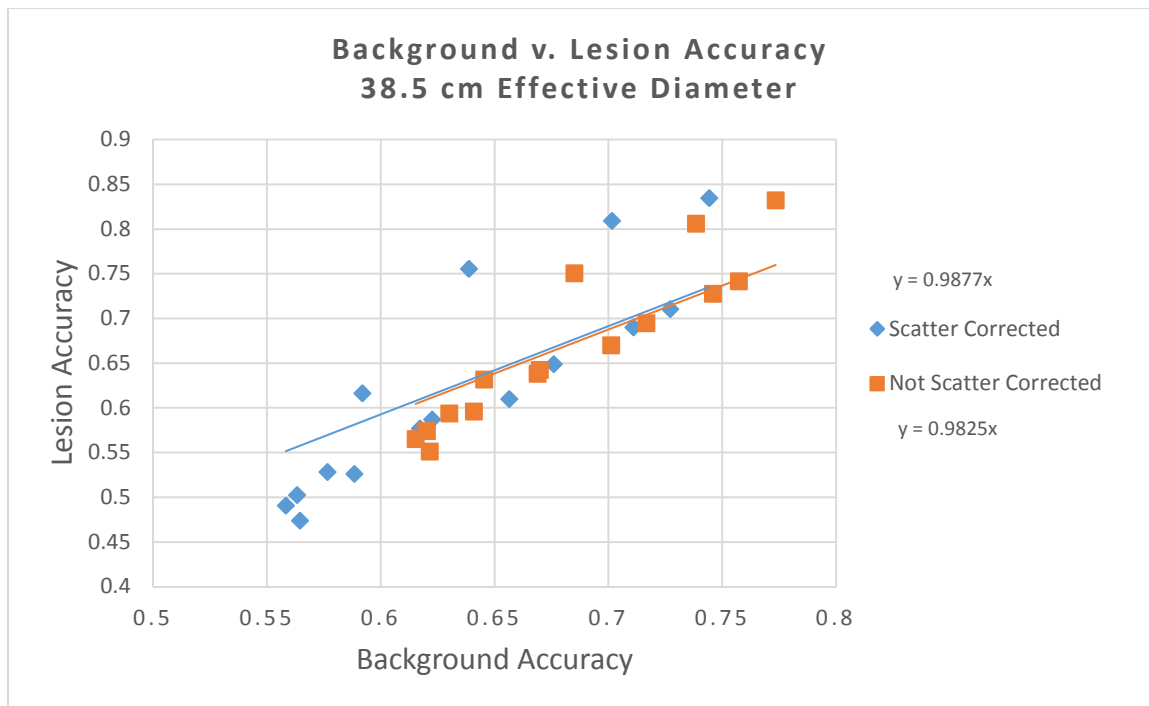


**Figure 12: Correlation of background accuracy to lesion accuracy for PET simulations of phantom effective diameter 38.5 cm using erroneous attenuation correction.**

### 3.1.3 Non-uniform PET with Scatter Correction Errors

For correctly attenuated but incorrectly scatter corrected simulated PET reconstructions, the 8:1 contrast had lower variability than the 1:1 contrast implying that scatter affects low uptake areas more. This result is expected due to the additive nature of scatter being a larger percentage of the total counts in a low uptake area.

**Table 11: Percent Variability over PET Lesion and Background ROI Mean due to Scatter Correction Errors for multiple phantom sizes.**

|                         | Effective Diameter |       |         |        |         |       |
|-------------------------|--------------------|-------|---------|--------|---------|-------|
|                         | 21.9 cm            |       | 31.7 cm |        | 38.5 cm |       |
| Scatter Profile Scaling | 8:1                | 1:1   | 8:1     | 1:1    | 8:1     | 1:1   |
| 70%                     | 0.23%              | 1.93% | 0.91%   | 12.53% | 0.21%   | 7.39% |
| 80%                     | 0.16%              | 1.25% | 0.57%   | 5.32%  | 0.13%   | 4.16% |
| 90%                     | 0.11%              | 0.63% | 0.29%   | 2.04%  | 0.09%   | 1.81% |
| 100%                    | 0.09%              | 0.13% | 0.08%   | 0.18%  | 0.08%   | 0.08% |
| 110%                    | 0.12%              | 0.53% | 0.22%   | 1.10%  | 0.11%   | 1.39% |
| 120%                    | 0.17%              | 1.03% | 0.41%   | 1.96%  | 0.14%   | 2.53% |
| 130%                    | 0.24%              | 1.51% | 0.59%   | 2.60%  | 0.18%   | 3.47% |

Figures 13-15 show plots of the regression analysis used to determine if error in a lesionless reconstruction implies similar error on lesions. Lesion error was more severe than background error in all three phantom sizes. The bias caused by the under and overcorrection of scatter effects the error of the background more than the lesions. In every case examined under correcting for scatter lead to an overestimation of lesion error while over correcting lead to an underestimation of lesion error. The quality of the lesion error estimation worsened with increasing phantom size.

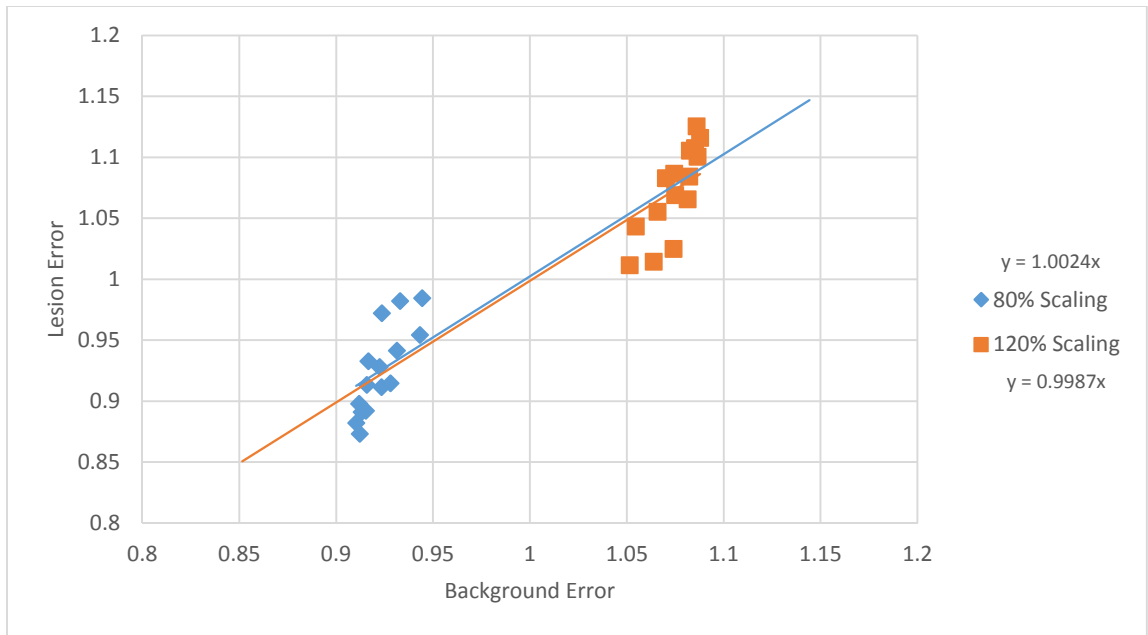


**Figure 13: Correlation of background error to lesion error for PET simulations of phantom effective diameter 21.9 cm using erroneous scatter correction.**

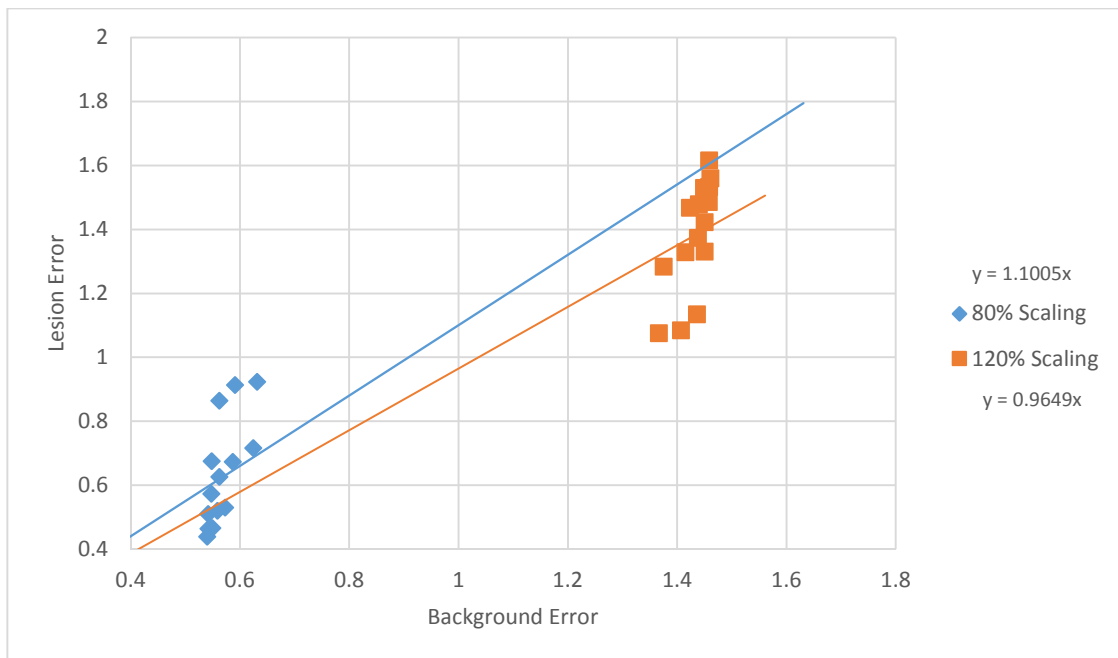


**Figure 14: Correlation of background error to lesion error for PET simulations of phantom effective diameter 31.7 cm using erroneous scatter correction.**



**Figure 15: Correlation of background error to lesion error for PET simulations of phantom effective diameter 38.5 cm using erroneous scatter correction.**

### 3.2 Physical Whole Body Phantom

The measured lesion ratios for the phantom when the best attenuation correction was applied were 7.29:1 and 4.48:1 for the scatter corrected and non-scatter corrected reconstructions, respectively. These values are less than expected based on pre-scan measurement of activity, possibly due to the uncertainty in the volume of the phantom when the pegboard and bottles are present and limited iterations. As shown in Tables 10-11, the variability decreased slightly with increasing tube-current and was at least twice as high in the background in every tested case. On-lesion variability for scatter corrected PET reconstructions was between 1.52% and 6.13% while off lesion the variability ranges from 10.00% to 18.26%. Similarly with the non-scatter corrected reconstructions variability ranged from 1.75% to 5.53% for on-lesion and 7.27% to 10.85% for off-lesion.

**Table 12: Percent variability over lesion locations using scatter correction and various attenuation corrections.**

| Scan Parameters  | 7.29:1 | 1:1    |
|------------------|--------|--------|
| 4 mAs - 80 kVp   | 6.13%  | 18.26% |
| 4 mAs - 120 kVp  | 3.18%  | 11.78% |
| 10 mAs - 120 kVp | 1.79%  | 10.23% |
| 48 mAs - 120 kVp | 1.52%  | 10.00% |

**Table 13: Variability over lesion locations using no scatter correction and various attenuation corrections.**

| Scan Parameters  | 7.29:1 | 1:1    |
|------------------|--------|--------|
| 4 mAs - 80 kVp   | 5.53%  | 10.85% |
| 4 mAs - 120 kVp  | 2.57%  | 7.27%  |
| 10 mAs - 120 kVp | 1.75%  | 8.92%  |
| 48 mAs - 120 kVp | 2.03%  | 10.09% |

As shown in Figures 16-18, the overall correlation shows that a low-error uniform PET implies that quantitation of hot lesions will have similar error, and that hot lesion quantitation is harmed with poor attenuation correction. The background error from the center of the phantom was the worst in every case, but the lesion error remains similar to other locations.

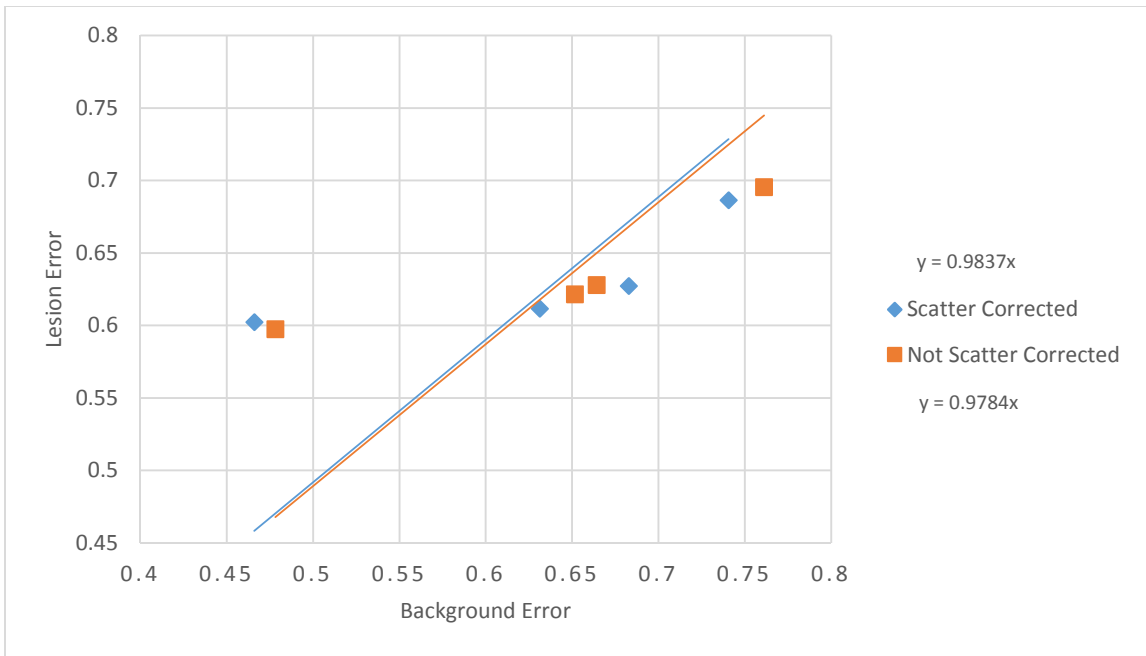


**Figure 16: Correlation of background error to lesion error for the physical phantom using CT with 80 kVp and 4 mAs.**

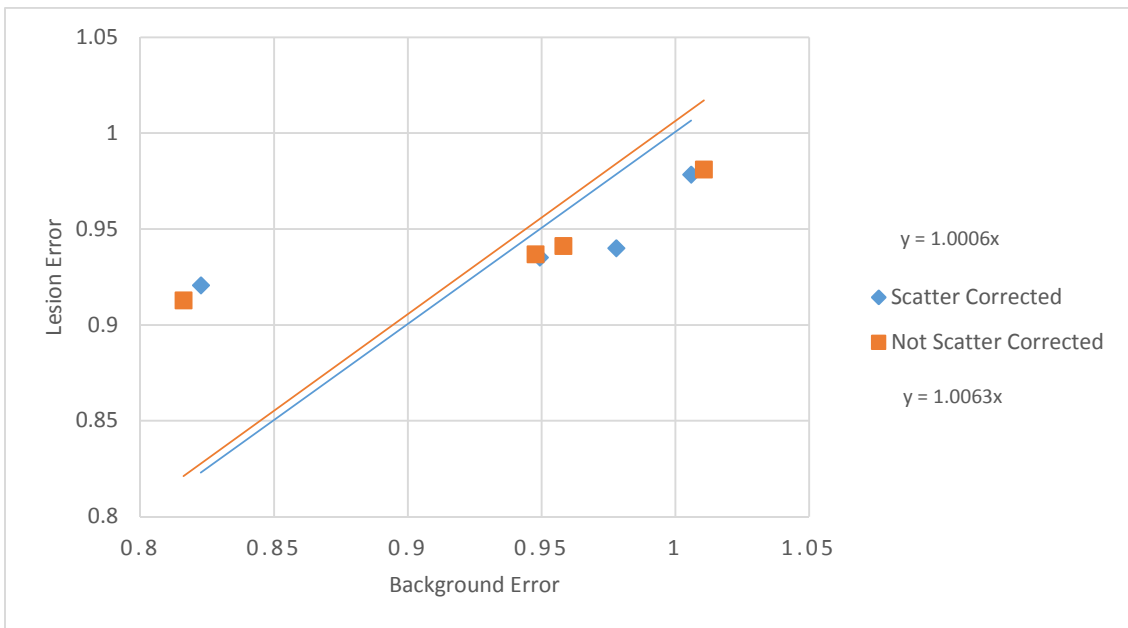


**Figure 17: Correlation of background error to lesion error for the physical phantom with 120 kVp and 4 mAs.**

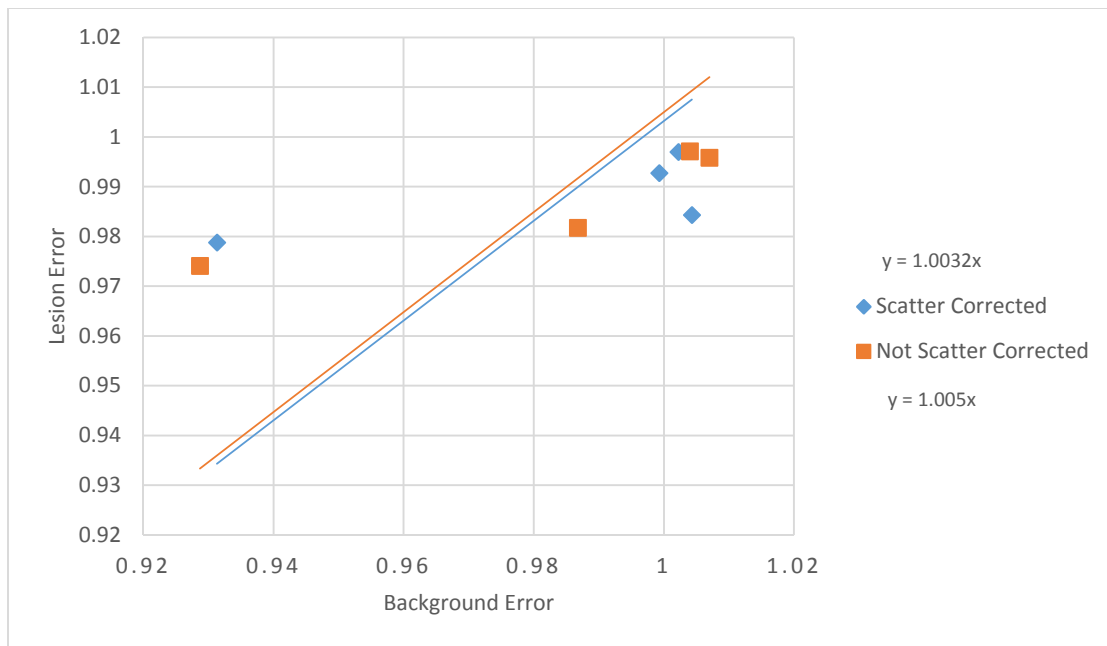


**Figure 18: Correlation of background error to lesion error for the physical phantom using CT with 120 kVp and 10 mAs.**

For the TOF versus nonTOF reconstructions, the variability was less than 1% on lesion and 15% in background as shown in Table 14. The background variability is once again greater than variability of lesions.

**Table 14: Percent variability over lesion locations using TOF and nonTOF reconstructions.**

|        | 8:1   | 1:1    |
|--------|-------|--------|
| TOF    | 0.63% | 14.34% |
| NonTOF | 0.51% | 13.19% |

## 4 Discussion

In these simulations and measurements, the overall quantitative accuracy of PET was most negatively affected by gross underestimation of the tube current needed while performing a CT scan. Many of the PET scans performed clinically at Duke are accompanied by a diagnostic or near diagnostic quality CT. Tube-currents of 300 mAs can be used in those exams by modulated tube current algorithm, which places them well within a margin of 5% error. ACR accreditation for a CT scanner requires that water in a 20 cm diameter cylindrical phantom be assigned the value  $0\pm 7$  HU. While that phantom is substantially smaller than the one scanned in this study or an actual patient, the image quality characteristics remain constant over body size when using modulated tube-current.

The lower minimum tube-current required to achieve uniformity in the physical phantom compared to simulation was most likely due to its smaller effective diameter. The physical phantom is more elongated than the tapering phantom despite having the type of geometry. With similar major axis lengths, the entire difference comes from the minor axis, which makes the center of the simulation phantom further from the surface. Thus it requires a higher initial flux of photons to avoid detector noise and give proper sampling of the attenuation coefficients.

Another technique that may provide interesting addition to this work is the use of raw CT data smoothing. Applying a low pass filter to the raw CT data to remove the

non-positive values instead of biasing the data allows it to be reconstructed and used for attenuation correction while lowering the required dose [8].

An earlier study investigated the use of modulated tube-current in CT scans used only for attenuation correction in PET found that a NI of 70 at 120 kVp and 140 kVp was sufficient to maintain quantitative PET accuracy within 5%, while this study's results show that a NI of 50 with 120 or 140 kVp is required [2]. This disparity is most likely due to the difference in applied ROI size. Their study used a 10 cm diameter circular ROI while a 4.9 cm diameter circular ROI was used in this study. Both ROIs were placed at the center of the phantom. While a larger ROI includes more data points, it is less sensitive to the errors induced at the center of the phantom where errors being measured are largest.

An interesting potential area of research is the uniformity of a non-attenuation corrected body using TOF. If scatter correction is done using a method that does not require a CT, such as by delayed events, there is a potential for lower dose PET acquisitions where only a planar scout x-ray for patient positioning is required. While this may never become a clinical practice with the popularity and usefulness of CT, it is certainly worth investigation.

This work may be extended in several ways. The fillable tapering phantom could be used to further investigate the results of simulation [3]. A more robust system of scatter estimation and correction, such as a Monte Carlo simulation or size dependent

scatter fraction, would provide more realistic scatter estimation. Simulations with no attenuation at all could be conducted to determine if a poor attenuation correction is better or worse than no correction at all. The examination of cold lesions or multiple hot lesions could be a stepping-stone toward a more realistic phantom setup.

## 5 Conclusion

As expected, effects of poor corrections can easily hurt quantitative accuracy in PET. CT based attenuation correction is a powerful tool to improve the accuracy of PET, but it must be used with sufficient parameters so that patient scans may be interpreted correctly. The errors in PET quantitation near the center of the body due to biased CT can become very large if insufficient flux is used. Using a modulated current algorithm can alleviate this issue, but errors in quantitative accuracy can still occur as the purpose of the algorithm is noise control, not quantitative accuracy. The largest problems occur as body size increases, which is of great concern when more than a third of US adults are obese [9]. With obesity linked to the incidence of many types of cancer, patients receiving a PET/CT are also more likely to be obese.

In simulation and measurements of the physical phantom, variability in across the body was always worse in background measurements than on hot lesions. This implies that variability measurements in a uniform phantom are a worst case scenario and that variability will be better than that measurement. Errors in background due to attenuation correction tend to overestimate errors in hot lesions, so measuring error in background is again a worst case scenario. Errors in background due to under and overcorrected scatter lead to an over and underestimate of hot lesion errors, respectively.

## References

- [1] General Electric Healthcare. (n.d.). Retrieved from [http://www3.gehealthcare.co.uk/~/media/documents/us-global/education/education/product-education-clinical/tip-app-library/gehealthcare-education-tip-app-library\\_ct-automa-smartma-theory.pdf](http://www3.gehealthcare.co.uk/~/media/documents/us-global/education/education/product-education-clinical/tip-app-library/gehealthcare-education-tip-app-library_ct-automa-smartma-theory.pdf)
- [2] Turkington TG, et al. (2011). Use of Tube-current Modulation to Minimize Radiation Dose in CT-based PET Attenuation Correction. *J Nucl Med*, 52, 52.
- [3] Wilson JM, et al. (2011). Development of a Fillable, Tapered PET/CT Phantom. *IEEE Transactions on Nuclear Science*, 58 (3), 651-659.
- [4] Wilson JM, et al. (2009). TOF-PET small-lesion image quality measured over a range of phantom sizes. *IEEE Nuclear Science Symposium Conference Record*, 3710-3714.
- [5] M Bergström, et al (1983). Correction for Scattered Radiation in a Ring Detector Positron Camera by Integral Transformation of the Projections. *Journal of Computer Assisted Tomography*, 42-50.
- [6] Wilson, JW. Parameterizing Image Quality of TOF versus Non-TOF PET as a Function of Body Size. 74-75.
- [7] Lokitz SJ, et al. (2007). Development of a phantom to simulate a wide range of body sizes. *Nuclear Science Symposium Conference Record*, 5, 3713-3717.
- [8] Colsher JG, et al (2008). Ultra Low Dose CT for Attenuation Correction in PET/CT. *Nuclear Science Symposium Conference Record*, 5506-5511.
- [9] Ogden CL, et al. (2014). Prevalence of Childhood and Adult Obesity in the United States, 2011-2012. *JAMA* (806-814).